

Anisotropic hybridization in CeRhSn


Thomas U. Böhm¹, Nicholas S. Sirica^{1,2}, Bo Gyu Jang^{1,3}, Yu Liu¹, Eric D. Bauer¹,
Yue Huang¹, Christopher C. Homes⁴, Jian-Xin Zhu¹, and Filip Ronning¹

¹*Los Alamos National Laboratory, Los Alamos, New Mexico 87545, USA*

²*U.S. Naval Research Laboratory, Washington DC 20375, USA*

³*Department of Advanced Materials Engineering for Information and Electronics, Kyung Hee University, Yongin 17104, Republic of Korea*

⁴*National Synchrotron Light Source II, Brookhaven National Laboratory, Upton, New York 11973, USA*

 (Received 3 June 2024; revised 7 August 2024; accepted 23 August 2024; published 12 September 2024)

The optical conductivity $\sigma(\omega, T)$ of CeRhSn was studied by broadband infrared spectroscopy. Temperature-dependent spectral weight transfer occurs over high energy (0.8 eV) and temperature (~ 500 K) scales, classifying CeRhSn as a mixed-valent compound. The optical conductivity reveals a substantial anisotropy in the electronic structure. Renormalization of $\sigma(\omega, T)$ occurs as a function of temperature to a coherent Kondo state with concomitant effective mass generation. Associated spectroscopic signatures were reproduced remarkably well by the combination of density functional theory and dynamical mean-field theory using a momentum-independent self-energy. The theory shows that the anisotropy for energies > 10 meV is mainly driven by the bare three-dimensional electronic structure that is renormalized by local electronic correlations. The possible influence of magnetic frustration and quantum criticality is restricted to lower energies.

DOI: [10.1103/PhysRevB.110.L121107](https://doi.org/10.1103/PhysRevB.110.L121107)

Quantum phase transitions in lanthanide- and actinide-based heavy fermions are some of the most widely studied phenomena in condensed matter physics [1–6]. Here, varying the hybridization strength between localized f - and delocalized conduction electrons (c) allows for the continuous tuning between strongly f - c hybridized Kondo and weakly hybridized magnetic states through the use of nonthermal control parameters such as pressure, chemical composition, or magnetic field. Within this canonical description of quantum criticality for f -block materials [7], mixed-valent compounds are frequently overlooked as the energy scale for valence fluctuations dominates over the low-energy competition between magnetic order and Kondo screening, leading to the emergence of many-body Kondo singlet states at a characteristically high temperature (> 100 K) [8–10]. However, the introduction of geometric frustration and/or reduced dimensionality between Kondo ions adds another dimension to the global magnetic phase diagram of f -electron materials [11–13], providing an alternate route to realize quantum criticality, even in the mixed-valent compounds [14–16].

The $CeTX$ (T = transition metal, X = p -block element) family of intermetallics is a promising material class for investigating such an interplay between geometric frustration and Kondo screening in a mixed-valent compound [1]. Here, Ce atoms sit on the distorted kagome lattice of a hexagonal ZrNiAl-type ($P\bar{6}2m$) structure depicted in Fig. 1(a). Of the members in this family, CeRhSn has attracted significant attention due to the rich variety of physical properties exhibited by this compound, including mixed valency [17–19], geometric frustration, quantum criticality [16,20], and strong magnetic and electronic anisotropy [10]. Ising-like susceptibilities $\chi_c \approx 10\chi_a$ at low temperatures naively contradict the mixed-valent behavior, which would lead to near equally

populated crystal-field levels. Meanwhile, resistivity measurements reveal signatures of Kondo coherence in the ab plane that are notably absent along the crystallographic c axis, suggesting an anisotropic mass renormalization in momentum space. Such behavior is at odds with the majority of mixed-valent compounds [21,22], whose isotropic, cubic symmetry often support a Fermi-liquid ground state, and emphasizes the impact that reduced dimensionality and magnetic frustration may have on Kondo coherence.

We perform Fourier transform infrared (FTIR) spectroscopy complemented by density functional theory (DFT) plus dynamical mean-field theory (DMFT) [23–25]. Experimentally, a polarization-dependent measurement separates the a - and the c -axis optical conductivity σ_{aa} and σ_{cc} . Emergent spectroscopic features indicate a transition from a high-temperature state with fluctuating local moments to a low-temperature coherent anisotropic Kondo state, governed by the screening of f -electron moments by conduction electrons. Their hybridization leads to an energy gap which introduces a multitude of new interband absorption channels at infrared energy scales, directly observable by our experiment [26]. It also yields flat bands populated with heavy fermions, where intraband transitions appear as a Drude peak and provide information on the mass enhancement and scattering rate [27]. The three-dimensional multiband electronic structure, however, complicates a conclusive analysis from the experiment alone. Therefore, we applied DFT+DMFT to resolve the spectroscopically observed features. Based on a momentum-independent self-energy from localized f states, we gain insight into the mechanism of hybridization and effective mass enhancement. We find that the anisotropy in the optical conductivity can be reproduced by applying local Kondo physics to the framework of an intrinsically anisotropic electronic structure reflected in the DFT.

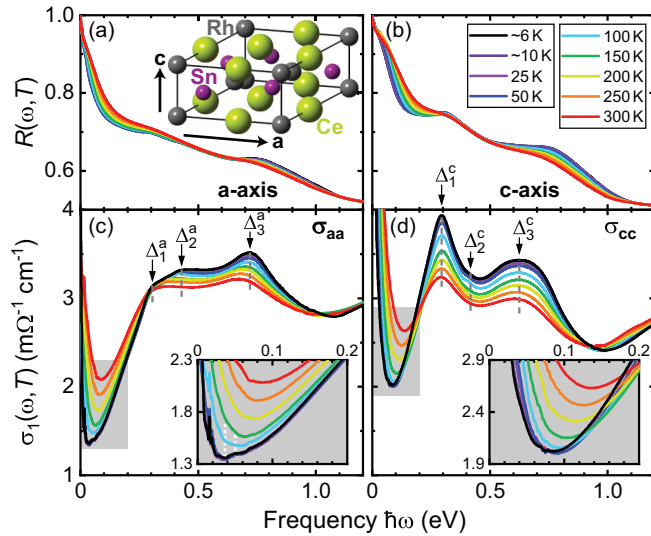


FIG. 1. Experimental results for CeRhSn. The reflectivity $R(\omega, T)$ in (a) and (b) and real optical conductivity $\sigma_1(\omega, T)$ in (c) and (d) are plotted as a function of frequency and temperature. (a) and (c) compile the spectra for a polarization applied along the a axis, and (b) and (d) for a polarization along c . The insets of (c) and (d) enlarge the spectra inside the gray-shaded boxes. Dashed white lines indicate the minimum ω_{\min} and shoulder ω_s developing at low temperatures. Narrow features below the minimum are optical phonon modes. The color coding for the temperatures is preserved for all experimental data throughout this Letter. The Supplemental Material provides data in the full frequency range up to 2.7 eV [29].

Experimentally, single-crystal CeRhSn was grown via the Czochralski method [28] in a tri-arc furnace under high-purity argon atmosphere [10]. The orientation of the as-cast single-crystalline rod was determined by means of Laue diffraction and verified within our experiments by using infrared-active optical phonons as a spectroscopic indicator for lattice orientation [29]. Such characterization demonstrates this sample to be single grain throughout the measured ac plane. Reflectivity experiments were performed at near normal incidence ($<15^\circ$) by applying linearly polarized light parallel to the crystallographic a and c axes [30]. We obtained the reflectivity spectra as displayed in Figs. 1(a) and 1(b), respectively. The optical conductivity $\sigma(\omega, T)$ was determined from the experimental reflectivity spectra by way of a Kramers-Kronig transform [29,31–33]. This yields the real parts of the optical conductivity tensor elements $\sigma_{aa}(\omega, T)$ and $\sigma_{cc}(\omega, T)$ as presented in Figs. 1(c) and 1(d), respectively. Details of the experiment and analysis are described in the Supplemental Material [29].

We observe that both directions of the optical conductivity σ_{aa} and σ_{cc} have a clear dip around 0.1 eV followed by three broad but distinct midinfrared (MIR) peaks labeled Δ_i [as marked in Figs. 1(c) and 1(d)] that extend from 0.2 up to 0.8 eV. The peak at Δ_2 becomes visible below 150 K. The energies of Δ_1 , Δ_2 , and Δ_3 are similar for both directions, while the intensities of these features are clearly anisotropic as could be expected for interband transitions in a hexagonal crystal. The most striking aspect of the data is a shift of spectral weight from low to high energies with decreasing

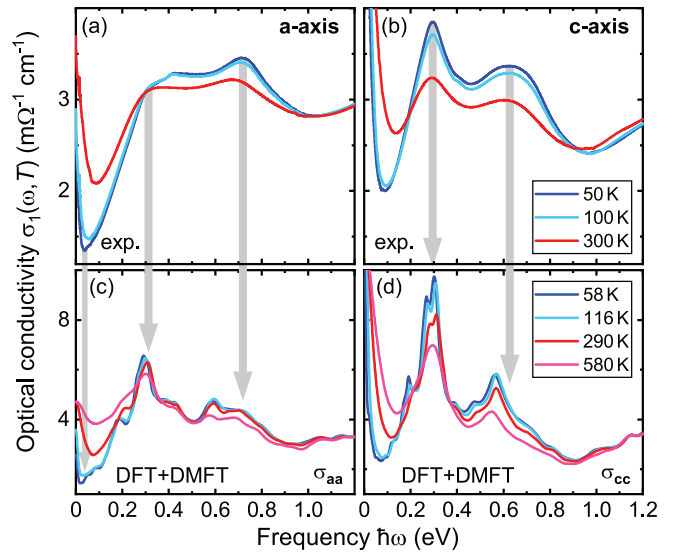


FIG. 2. Comparison of experimental optical conductivity with theoretically computed optical conductivity. (a) and (c) duplicate the optical conductivity of Fig. 1 for a subset of temperatures, where nearby theoretical calculations, shown in (b) and (d), are available. Gray arrows mark significant experimentally determined peak positions and the minimum in (a) for the lowest temperature.

temperature. In general, a shift of spectral weight is a clear signature of an energy gap Δ with optically induced transitions of quasiparticles across the gap. The transfer of spectral weight to high energies is more prominent in σ_{cc} than in σ_{aa} . The spectral weight transfer does not saturate at room temperature. Rather, an extrapolation of the continuing spectral weight loss gives a temperature scale of 500 ± 100 K [29], which we identify as the single-ion Kondo scale. In contrast, low-energy features are more striking in σ_{aa} than in σ_{cc} . A new minimum at $\omega_{\min} = 35$ meV, followed by a shoulder at $\omega_s = 50$ meV develops at 100 K only for σ_{aa} , and is most pronounced and saturated for $T \leq 50$ K (Fig. 1 insets).

To elucidate the origin of the spectral weight transfer and observed anisotropies in the optical conductivity we have performed electronic structure calculations by fully charge self-consistent DMFT, combined with DFT [25] using the WIEN2K code [34]. The Perdew-Burke-Ernzerhof generalized gradient approximation (PBE-GGA) was employed for the exchange-correlation potential [35]. Electronic correlation effects of Ce $4f$ orbitals were treated by a momentum-independent (local) self-energy from the DMFT part with a continuous-time quantum Monte Carlo (CTQMC) solver [24]. Hubbard parameters $U = 5$ eV and $J = 0.7$ eV were used. The optical conductivity was computed with the formalism presented in Ref. [25] (see Supplemental Material for details [29]). A comparison of the experimentally measured and theoretically calculated optical conductivity is presented in Fig. 2. Remarkable similarities are apparent. The previously described peak structure and spectral weight shift, which is more pronounced in σ_{cc} , is by and large captured by the theory. The more pronounced minimum in σ_{aa} at low temperatures/energies is also captured by the theory. The good agreement implies that the observed

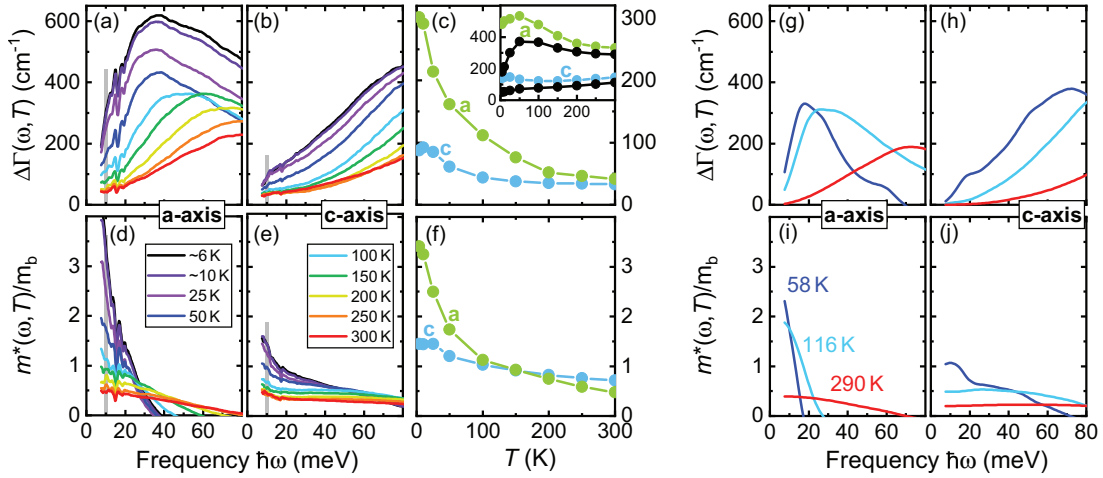


FIG. 3. Extended Drude analysis for the scattering rate and effective mass. (a) and (b) show the relative scattering rates for the a and c axis, and (d) and (e) the effective mass, respectively. Averaged values from 9 to 11 meV are compiled as a function of temperature in (c) and (f). The inset of (c) depicts absolute values of the averaged scattering rate $\Gamma(9\text{--}11\text{ meV}, T)$ along with $\Gamma_0(T)$ (black) from Ref. [10]. (g)–(j) are the respective results, obtained from theoretically computed optical conductivity σ_{aa} and σ_{cc} shown in Figs. 2(c) and 2(d).

temperature-dependent anisotropies stem from a renormalization of the electronic structure that is local in real space, yielding a momentum-independent self-energy that is captured within the DMFT framework.

We now turn our attention to the lowest energies accessible by our experiment to gain insight on the dynamics of the heavy fermion state. Analyzing the data using an extended Drude model enables the extraction of a frequency-dependent scattering rate $\Gamma(\omega, T) = \omega_p^2 / (4\pi) \text{Re}[1/\sigma(\omega, T)]$ and effective mass $m^*(\omega, T)/m_b = -\omega_p^2 / (4\pi\omega) \text{Im}[1/\sigma(\omega, T)]$, with the bare band mass m_b [27]. The plasma frequency ω_p is given by the carrier density through the optical conductivity sum rule. A precise value is difficult to determine due to the presence of interband transitions. We chose $\omega_p = 1\text{ eV}$ and note that a different value will only scale our results described below, as we limit our analysis to systematic trends that are independent of the precise value of the plasma frequency. Figures 3(a)–3(c) show $\Delta\Gamma = \Gamma - \Gamma_0$ with the zero-frequency scattering rate $\Gamma_0(T) = \omega_p^2 / (4\pi) \rho_{dc}(T)$. The difference allows for a better view of the frequency dependence beyond ρ_{dc} . The results for the effective mass m^* are shown in Figs. 3(d)–3(f). The effective mass is strongly frequency and temperature dependent in the low-energy limit ($\lesssim 40\text{ meV}$), which is consistent with strong electronic renormalization observed in transport and thermodynamic measurements [10,17]. We obtain increasingly larger scattering rates and effective masses in the ab plane than along the c axis with decreasing temperature. Comparable values at 300 K turn into a disproportional growth in the ab plane particularly below $\sim 150\text{ K}$, reaching $\Delta\Gamma_a = 3.3\Delta\Gamma_c$ and $m_a^* = 2.4m_c^*$ at $\sim 6\text{ K}$. This anisotropy is consistent with the previous observation that the minimum in the optical conductivity is driven to lower energies for the ab -plane data relative to the c -axis data.

As mentioned in the Introduction, CeRhSn presents a confounding confluence of mixed-valent energy scales, strongly anisotropic low-temperature transport, and thermodynamic

responses as well as quantum criticality, which raises the question as to what is the role of the reduced dimensionality and/or magnetic frustration present in the Ce lattice of this compound. In a simple mean-field picture of the Kondo lattice, a hybridization gap forms between the conduction bands and a renormalized heavy band [26,36]. Precisely such a hybridization gap is observed in the optical conductivity response of many Ce-lattice compounds [21,22,37–41]. In CeRhSn the dominant MIR peak occurs for the c -axis polarization at 0.3 eV, consistent with a previous report [42]. This energy scale is larger than other well-known mixed-valent compounds such as YbAl₃, CeSn₃, and CePd₃ [21,22], consistent with the mixed-valent classification for CeRhSn from other spectroscopic probes [17–19]. Furthermore, it is clear that the transfer of spectral weight will continue well above room temperature. Examining the temperature dependence of the spectral weight contained in the peaks suggests this spectral weight transfer will persist up to $500 \pm 100\text{ K}$ [29], giving a Kondo temperature similar to other mixed-valent compounds.

It is notable that the spectral weight transfer extends to energies as large as 0.8 eV, with a clear second subdominant peak near 0.6 eV, and a strongly anisotropic response between the a - and c -axes conductivity. At first glance this could suggest a distribution of energy scales in either real or momentum space. These spectral features, however, are all reproduced in our DFT+DMFT calculations shown in Fig. 2. Single-site DMFT assumes a momentum-independent self-energy of the f electrons. The resulting anisotropy and the distribution of energy scales is thus a consequence of the underlying band structure. Each band and \mathbf{k} point will contribute differently to the directional-dependent conductivity based on matrix elements for the individual optical transitions, and each of those \mathbf{k} points/bands will have a different hybridization strength to the f orbital, which is responsible for the electronic renormalization. Thus, the renormalization of CeRhSn's electronic structure at high energies appears similar to other

mixed-valent compounds, but with the added complexity of anisotropic f - c hybridization present in the band structure.

Concomitant with the formation of the hybridization gap, the low-frequency conductance will reflect the scattering of the conduction electrons off of the f moments. At high temperatures the scattering occurs off of individual f moments, while below the coherence temperature, there is a collective screening of the local moments and an associated mass enhancement of the quasiparticles at the Fermi energy. It is generally difficult to resolve the coherence temperature in spectroscopic measurements. Previous optical conductivity measurements on YbAl_3 have associated the emergence of a peak within the hybridization gap as a signature of lattice coherence [22]. We observe a similar shoulder in σ_{aa} at 50 meV, which emerges at 100 K—close to the coherence temperature of 70 K obtained from ρ_a [10]. It is interesting that this feature is not present in σ_{cc} where dc resistivity data are similarly found to lack a coherence peak for ρ_c .

The fact that a coherence peak is observed in ρ_a but not ρ_c suggests that the quasiparticles which dominate the c -axis transport have a significantly smaller hybridization to the f electrons than the quasiparticles contributing to the in-plane transport. This anisotropy is reflected in our extended Drude analysis. While the effective mass m^* and the frequency-dependent scattering rate $\Delta\Gamma$ are still enhanced in the c -axis conductivity data, the enhancement is at least twice as strong for the a -axis conductivity. Remarkably, performing the same extended Drude analysis on the theoretically computed optical conductivity reproduces the frequency and temperature dependence for both directions down to 10 meV [see Figs. 3(g)–3(j)]. This suggests that the anisotropic mass renormalization is fundamentally a property of the underlying band structure as well, which is renormalized through a momentum-independent self-energy of the f electrons.

We have illustrated that the electronic structure and the renormalization thereof in CeRhSn is strongly anisotropic and spans energy scales up to 0.8 eV, confirming CeRhSn

as a mixed-valent material. Despite the presence of magnetic frustration in the Ce lattice, the anisotropy of the renormalization and the energy scales can be well accounted for from first-principles calculations using a DFT+DMFT framework, which assumes a momentum-independent self-energy. Several mysteries in CeRhSn remain. Notably, it is highly counterintuitive to observe a strongly anisotropic spin susceptibility in a mixed-valent compound for which no high-energy crystal field excitations have been identified [43]. Also surprising is the observation of the non-Fermi-liquid behavior at low temperatures, which appears to be related to the presence of magnetic frustration [16]. Additional spectroscopic measurements to lower frequencies would be interesting to clarify the origins of these puzzles.

Note added. Recently, we became aware of a related work [44]. The optical conductivity data are in very good agreement with ours though the focus of their manuscript is different.

We thank Ken Burch, Peter Armitage, Ken O’Neal, and Rohit Prasankumar for enlightening discussions to improve our FTIR spectroscopy effort. Work at Los Alamos was carried out under the auspices of the U.S. Department of Energy (DOE) National Nuclear Security Administration (NNSA) under Contract No. 89233218CNA000001. The experimental work acknowledges support from the DOE Office of Basic Energy Sciences, Materials Sciences and Engineering Division. The theoretical calculations were performed with support from LANL LDRD Program with project XXYU and XXNV. The work was in part supported by Center for Integrated Nanotechnologies, a DOE BES user facility, in partnership with the LANL Institutional Computing Program for computational resources. This research used the Infrared Lab of the National Synchrotron Light Source II, a U.S. DOE Office of Science User Facility operated for the DOE Office of Science by Brookhaven National Laboratory under Contract No. DE-SC0012704.

-
- [1] R. Pöttgen and B. Chevalier, Cerium intermetallics with ZrNiAl-type structure—a review, *Z. Naturforsch. B* **70**, 289 (2015).
 - [2] O. Janka, O. Niehaus, R. Pöttgen, and B. Chevalier, Cerium intermetallics with TiNiSi-type structure, *Z. Naturforsch. B* **71**, 737 (2016).
 - [3] R. Pöttgen, O. Janka, and B. Chevalier, Cerium intermetallics CeTX – review III, *Z. Naturforsch. B* **71**, 165 (2016).
 - [4] S. Kirchner, S. Paschen, Q. Chen, S. Wirth, D. Feng, J. D. Thompson, and Q. Si, Colloquium: Heavy-electron quantum criticality and single-particle spectroscopy, *Rev. Mod. Phys.* **92**, 011002 (2020).
 - [5] H. v. Löhneysen, A. Rosch, M. Vojta, and P. Wölfle, Fermi-liquid instabilities at magnetic quantum phase transitions, *Rev. Mod. Phys.* **79**, 1015 (2007).
 - [6] Q. Si and F. Steglich, Heavy fermions and quantum phase transitions, *Science* **329**, 1161 (2010).
 - [7] S. Doniach, The Kondo lattice and weak antiferromagnetism, *Physica B+C* **91**, 231 (1977).
 - [8] Y. Shimura, A. Wörl, M. Sundermann, S. Tsuda, D. T. Adroja, A. Bhattacharyya, A. M. Strydom, A. D. Hillier, F. L. Pratt, A. Gloskovskii, A. Severing, T. Onimaru, P. Gegenwart, and T. Takabatake, Antiferromagnetic correlations in strongly valence fluctuating CeIrSn, *Phys. Rev. Lett.* **126**, 217202 (2021).
 - [9] A. L. Cornelius, J. M. Lawrence, T. Ebihara, P. S. Riseborough, C. H. Booth, M. F. Hundley, P. G. Pagliuso, J. L. Sarrao, J. D. Thompson, M. H. Jung, A. H. Lacerda, and G. H. Kwei, Two energy scales and slow crossover in YbAl_3 , *Phys. Rev. Lett.* **88**, 117201 (2002).
 - [10] M. S. Kim, Y. Echizen, K. Umeo, S. Kobayashi, M. Sera, P. S. Salamkha, O. L. Sologub, T. Takabatake, X. Chen, T. Tayama, T. Sakakibara, M. H. Jung, and M. B. Maple, Low-temperature anomalies in magnetic, transport, and thermal properties of single-crystal CeRhSn with valence fluctuations, *Phys. Rev. B* **68**, 054416 (2003).
 - [11] P. Coleman and A. H. Nevidomskyy, Frustration and the Kondo effect in heavy fermion materials, *J. Low Temp. Phys.* **161**, 182 (2010).

- [12] Q. Si, Global magnetic phase diagram and local quantum criticality in heavy fermion metals, *Phys. B: Condens. Matter* **378-380**, 23 (2006).
- [13] H. Zhao, J. Zhang, M. Lyu, S. Bachus, Y. Tokiwa, P. Gegenwart, S. Zhang, J. Cheng, Y.-F. Yang, G. Chen, Y. Isikawa, Q. Si, F. Steglich, and P. Sun, Quantum-critical phase from frustrated magnetism in a strongly correlated metal, *Nat. Phys.* **15**, 1261 (2019).
- [14] Y. Matsumoto, S. Nakatsuji, K. Kuga, Y. Karaki, N. Horie, Y. Shimura, T. Sakakibara, A. H. Nevidomskyy, and P. Coleman, Quantum criticality without tuning in the mixed valence compound β -YbAlB₄, *Science* **331**, 316 (2011).
- [15] M. S. Grbić, E. C. T. O'Farrell, Y. Matsumoto, K. Kuga, M. Brando, R. KÜchler, A. H. Nevidomskyy, M. Yoshida, T. Sakakibara, Y. Kono, Y. Shimura, M. L. Sutherland, M. Takigawa, and S. Nakatsuji, Anisotropy-driven quantum criticality in an intermediate valence system, *Nat. Commun.* **13**, 2141 (2022).
- [16] Y. Tokiwa, C. Stingl, M.-S. Kim, T. Takabatake, and P. Gegenwart, Characteristic signatures of quantum criticality driven by geometrical frustration, *Sci. Adv.* **1**, e1500001 (2015).
- [17] A. Ślebarski, M. B. Maple, E. J. Freeman, C. Sirvent, M. Radłowska, A. Jezierski, E. Granado, Q. Huang, and J. W. Lynn, Strongly correlated electron behaviour in the compound CeRhSn, *Philos. Mag. B* **82**, 943 (2002).
- [18] M. Sundermann, A. Marino, A. Gloskovskii, C. Yang, Y. Shimura, T. Takabatake, and A. Severing, Quantitative investigation of the $4f$ occupation in the quasikagome Kondo lattice CeRh_{1-x}Pd_xSn, *Phys. Rev. B* **104**, 235150 (2021).
- [19] M. Gamża, A. Ślebarski, and H. Rosner, Electronic structure of CeRhX (X = Sn, In), *Eur. Phys. J. B* **67**, 483 (2009).
- [20] S. Kittaka, Y. Kono, S. Tsuda, T. Takabatake, and T. Sakakibara, Field-angle-resolved landscape of non-Fermi-liquid behavior in the quasi-kagome Kondo lattice CeRhSn, *J. Phys. Soc. Jpn.* **90**, 064703 (2021).
- [21] B. Bucher, Z. Schlessinger, D. Mandrus, Z. Fisk, J. Sarrao, J. F. DiTusa, C. Oglesby, G. Aeppli, and E. Bucher, Charge dynamics of Ce-based compounds: Connection between the mixed valent and Kondo-insulator states, *Phys. Rev. B* **53**, R2948 (1996).
- [22] H. Okamura, T. Michizawa, T. Nanba, and T. Ebihara, Pseudogap formation and heavy-carrier dynamics in intermediate-valence YbAl₃, *J. Phys. Soc. Jpn.* **73**, 2045 (2004).
- [23] B. G. Jang, K. R. O'Neal, C. Lane, T. U. Böhm, N. Sirica, D. Yarotski, E. D. Bauer, F. Ronning, R. Prasankumar, and J.-X. Zhu, One-dimensionality signature in optical conductivity of heavy-fermion CeIr₃B₂, *Phys. Rev. B* **107**, 205116 (2023).
- [24] K. Haule, Quantum Monte Carlo impurity solver for cluster dynamical mean-field theory and electronic structure calculations with adjustable cluster base, *Phys. Rev. B* **75**, 155113 (2007).
- [25] K. Haule, C.-H. Yee, and K. Kim, Dynamical mean-field theory within the full-potential methods: Electronic structure of CeIrIn₅, CeCoIn₅, and CeRhIn₅, *Phys. Rev. B* **81**, 195107 (2010).
- [26] S.-I. Kimura, Y. S. Kwon, C. Krellner, and J. Sichelschmidt, Optical evidence of local and itinerant states in Ce- and Yb-heavy-fermion compounds, *Electron. Struct.* **3**, 024007 (2021).
- [27] A. V. Puchkov, D. N. Basov, and T. Timusk, The pseudogap state in high- T_c superconductors: An infrared study, *J. Phys.: Condens. Matter* **8**, 10049 (1996).
- [28] J. Czochralski, Ein neues Verfahren zur Messung der Kristallisationsgeschwindigkeit der Metalle, *Z. Phys. Chem.* **92U**, 219 (1918).
- [29] See Supplemental Material at <http://link.aps.org/supplemental/10.1103/PhysRevB.110.L121107> for sample preparation, data analysis, and details of the experiment and theory.
- [30] C. C. Homes, M. Reedyk, D. A. Cradles, and T. Timusk, Technique for measuring the reflectance of irregular, submillimeter-sized samples, *Appl. Opt.* **32**, 2976 (1993).
- [31] D. B. Tanner, Use of x-ray scattering functions in Kramers-Kronig analysis of reflectance, *Phys. Rev. B* **91**, 035123 (2015).
- [32] B. L. Henke, E. M. Gullikson, and J. C. Davis, X-ray interactions: Photoabsorption, scattering, transmission, and reflection at $E = 50\text{--}30,000$ eV, $Z = 1\text{--}92$, *At. Data Nucl. Data Tables* **54**, 181 (1993).
- [33] E. M. Gullikson, CXRO X-Ray Interactions With Matter, https://henke.lbl.gov/optical_constants/ (1995).
- [34] P. Blaha, K. Schwarz, F. Tran, R. Laskowski, G. K. H. Madsen, and L. D. Marks, WIEN2k: An APW+lo program for calculating the properties of solids, *J. Chem. Phys.* **152**, 074101 (2020).
- [35] J. P. Perdew, K. Burke, and M. Ernzerhof, Generalized gradient approximation made simple, *Phys. Rev. Lett.* **77**, 3865 (1996).
- [36] J. H. Shim, K. Haule, and G. Kotliar, Modeling the localized-to-itinerant electronic transition in the heavy fermion system CeIrIn₅, *Science* **318**, 1615 (2007).
- [37] H. Okamura, M. Matsunami, T. Nanba, T. Suemitsu, T. Yoshino, T. Takabatake, Y. Isikawa, and H. Harima, Pseudogap formation in the optical spectra of CeNiSn, CeRhSb, and CeRhAs, *Phys. B: Condens. Matter* **312-313**, 218 (2002).
- [38] F. P. Mena, D. van der Marel, and J. L. Sarrao, Optical conductivity of CeMIn₅ ($M = \text{Co, Rh, Ir}$), *Phys. Rev. B* **72**, 045119 (2005).
- [39] S.-I. Kimura, Y. Muro, and T. Takabatake, Anisotropic electronic structure of the Kondo semiconductor CeFe₂Al₁₀ studied by optical conductivity, *J. Phys. Soc. Jpn.* **80**, 033702 (2011).
- [40] S.-I. Kimura, T. Iizuka, H. Miyazaki, T. Hajiri, M. Matsunami, T. Mori, A. Irizawa, Y. Muro, J. Kajino, and T. Takabatake, Optical study of charge instability in CeRu₂Al₁₀ in comparison with CeOs₂Al₁₀ and CeFe₂Al₁₀, *Phys. Rev. B* **84**, 165125 (2011).
- [41] R. Y. Chen and N. L. Wang, Infrared properties of heavy fermions: Evolution from weak to strong hybridizations, *Rep. Prog. Phys.* **79**, 064502 (2016).
- [42] H. Okamura, T. Watanabe, M. Matsunami, N. Nishihara, N. Tsujii, T. Ebihara, H. Sugawara, H. Sato, Y. Ōnuki, Y. Isikawa, M. S. Kim, T. Takabatake, and T. Nanba, Universal scaling in the optical conductivity of heavy fermion compounds, *Phys. B: Condens. Matter* **403**, 761 (2008).
- [43] H. Higaki, I. Ishii, D. Hirata, M.-S. Kim, T. Takabatake, and T. Suzuki, Elastic, thermal, magnetic and transport properties of Kondo compounds CeRhIn and CeRhSn, *J. Phys. Soc. Jpn.* **75**, 024709 (2006).
- [44] S.-I. Kimura, M. F. Lubis, H. Watanabe, Y. Shimura, and T. Takabatake, Anisotropic non-Fermi liquid and dynamical Planckian scaling of the quasi-kagome Kondo lattice CeRhSn, *arXiv:2402.18176*.